IMPACT OF ARRHENIUS ACTIVATION ENERGY IN VISCOELASTIC NANOMATERIAL FLOW SUBJECT TO BINARY CHEMICAL REACTION AND NON-LINEAR MIXED CONVECTION

by

Salman AHMAD [a*], ***Muhammad Ijaz KHAN*** [a], ***M. Waleed Ahmed KHAN*** [a], ***Tufail A. KHAN*** [b], ***Tasawar HAYAT*** [a,c], ***and Ahmed ALSAEDI*** [c]

[a] Department of Mathematics, Quaid-I-Azam University, Islamabad, Pakistan
[b] Department of Basic Sciences, University of Engineering and Technology, Peshawar, Pakistan
[c] Non-linear Analysis and Applied Mathematics (NAAM) Research Group, Faculty of Science, King Abdulaziz University, Jeddah, Saudi Arabia

Original scientific paper
https://doi.org/10.2298/TSCI180524212A

The computational investigations on mixed convection stagnation point flow of Jeffrey nanofluid over a stretched surface is presented herein. The sheet is placed vertical over which nanomaterials flowing upward direction. Arrhenius activation energy and binary chemical reaction are accounted. Non-linear radiative heat flux, MHD, viscous dissipation, heat source/sink, and Joule heating are considered. Initially the non-linear flow expressions are converted to ordinary one and then tackled for series solutions by homotopy analysis method. Consider flow problem are discussed for velocity, temperature and concentration through various flow variables. Furthermore, skin friction coefficient, Sherwood number, and heat transfer rate are computed graphically.

Key words: *activation energy, non-linear radiative heat flux, Jeffrey nanofluid, viscous dissipation and Joule heating*

Introduction

Studies of non-Newtonian fluids have great interest due to their wide range applications in various field like physiology, pharmaceutical, fiber technology, coating of wires, food products, crystal growth and so forth. Properties of non-Newtonian fluid cannot characterize by single constitutive relation. Therefore, various non-Newtonian fluid models have been proposed, see [1-14]. Generally, these models are divided into rate, differential and integral types. Here we focused on Jeffrey fluid model. Which is a rate type fluid model and it is describe both relaxation and retardation times behavior. Studies associated to Jeffrey fluid can be seen in [15-22].

Suspension of nanoscale sized particles in base fluid is known as nanofluid. Nanoparticles in base fluid used to improve thermal conductivity of base fluid. There are ample demands of nanofluids in various fields like medical, industries and engineering, *etc*. For heating and cooling purpose nanofluids used in industries, modern drug delivery system, electronic devices batteries and hyperthermia, *etc*. Heat transfer enhancement by nanoparticles was first addressed Choi [23] and Buongiorno [24] developed a model to describe thermal conductivity enhance-

* Corresponding author, e-mail: salmanuom206@gmail.com

ment in nanomaterials. He addressed seven slip phenomena *i. e*. Brownian diffusion, thermophoresis, Magnus, gravity, fluid drainage and inertia. He concluded that thermophoresis and Brownian diffusion are major ruling slip phenomena in the nanomaterials. Shekholeslami *et al*. [25] studies the impact of MHD on flow of CuO-water nanomaterials with mixed convection. Farooq *et al*. [26] disclosed influences of non-linear thermal radiation and MHD on stagnation point flow of viscoelastic nanofluid. Abbasi *et al*. [27] explored flow of nanomaterial over a moving surface. The effect of magnetic dipole on flow of Maxwell nanofluids is investigated by Hayat *et al*. [28]. Lin *et al.* [29] explored impact of MHD on flow of pseudo-plastic nanomaterial. Studies associated to nanofluid can be seen in [30-35].

The objective of this investigation is to examine the influences of activation energy, heat source/sink, viscous dissipation, Joule heating, magnetic field on non-linear mixed convective stagnation point flow of non-linear radiative Jeffrey nanofluids over a stretching sheet. Transformations procedure is implemented to transform the governing partial differential equations into ordinary ones. Series solution is pointed out by homotopy algorithm [36-38]. The outcome of flow variable on concentration, velocity, temperature, Sherwood number, Nusselt number and skin friction is analyzed and discussed through graphs.

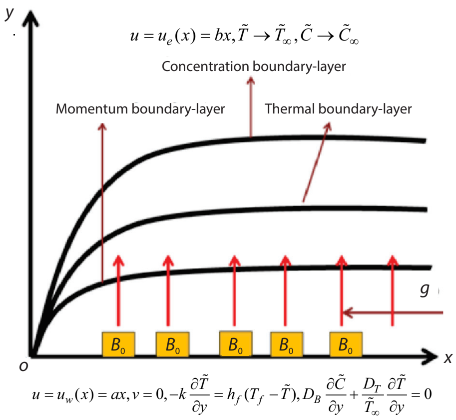

Figure 1. Systematic diagram

Modelling

Mixed convection stagnation point flow of Jeffrey nanofluid over a stretchable surface is investigated. Arrhenius activation energy and binary chemical reaction are considered. Electrically conducting fluid is considered. Energy equation is discussed in the presence of non-linear radiative heat flux and heat source/sink. Furthermore, dissipation and Joule heating are taken. Flow diagram is presented in fig. 1. The flow expressions [39]:

$$\frac{\partial \tilde{u}}{\partial x} + \frac{\partial \tilde{v}}{\partial y} = 0 \tag{1}$$

$$\tilde{u}\frac{\partial \tilde{u}}{\partial x} + \tilde{v}\frac{\partial \tilde{u}}{\partial y} = \tilde{u}_e\frac{\partial \tilde{u}_e}{\partial x} + \frac{\sigma B_0^2}{\rho}\left(\tilde{u}_e - \tilde{u}\right) + \frac{\nu}{1+\lambda_2}\left[\frac{\partial^2 \tilde{u}}{\partial y^2} + \lambda_1\left(\tilde{u}\frac{\partial^3 \tilde{u}}{\partial x \partial y^2} + v\frac{\partial^3 \tilde{u}}{\partial y^3} - \frac{\partial \tilde{u}}{\partial x}\frac{\partial^2 \tilde{u}}{\partial y^2} + \frac{\partial \tilde{u}}{\partial y}\frac{\partial^2 \tilde{u}}{\partial y^2}\right)\right]\cdot$$
$$\cdot g\left[\chi_1\left(\tilde{T} - \tilde{T}_\infty\right) + \chi_2\left(\tilde{T} - \tilde{T}_\infty\right)^2 + \chi_3\left(\tilde{C} - \tilde{C}_\infty\right) + \chi_4\left(\tilde{C} - \tilde{C}_\infty\right)^2\right] \tag{2}$$

$$\tilde{u}\frac{\partial \tilde{T}}{\partial x} + \tilde{v}\frac{\partial \tilde{T}}{\partial y} = \frac{k}{\rho c_p}\frac{\partial^2 \tilde{T}}{\partial y^2} - \frac{16\sigma}{3k\rho c_p}\frac{\partial}{\partial y}\left(\tilde{T}^3\frac{\partial \tilde{T}}{\partial y}\right) + \tau\left[D_B\left(\frac{\partial \tilde{C}}{\partial y}\frac{\partial \tilde{T}}{\partial y}\right) + \frac{D_T}{\tilde{T}_\infty}\left(\frac{\partial T}{\partial y}\right)^2\right] + \frac{Q_0}{\rho c_p}\left(\tilde{T} - \tilde{T}_\infty\right) +$$
$$+ \frac{\sigma B_0^2}{\rho c_p}\tilde{u}^2 + \frac{\mu}{\rho c_p(1+\lambda_2)}\left[\left(\frac{\partial \tilde{u}}{\partial y}\right)^2 + \lambda_1\left(\tilde{u}\frac{\partial \tilde{u}}{\partial y}\frac{\partial^2 \tilde{u}}{\partial x \partial y} + v\frac{\partial \tilde{u}}{\partial y}\frac{\partial^2 \tilde{u}}{\partial y}\right)\right] \tag{3}$$

$$\tilde{u}\frac{\partial \tilde{C}}{\partial x} + \tilde{v}\frac{\partial \tilde{C}}{\partial y} = D_B\frac{\partial^2 \tilde{C}}{\partial y^2} + \frac{D_T}{\tilde{T}_\infty}\frac{\partial^2 \tilde{T}}{\partial y^2} - k_r^2\left(\tilde{C} - \tilde{C}_\infty\right)\left(\frac{\tilde{T}}{\tilde{T}_\infty}\right)^n \exp\left(-\frac{E_a}{\kappa \tilde{T}}\right) \tag{4}$$

with

$$\tilde{u}=u_w(x)=ax,\ \tilde{v}=0,\ -k\frac{\partial\tilde{T}}{\partial y}=h_f\left(\tilde{T}_w-\tilde{T}\right),\ D_B\frac{\partial\tilde{C}}{\partial y}+\frac{D_T}{\tilde{T}_\infty}\frac{\partial\tilde{T}}{\partial y}=0\text{ at }y=0$$
$$\tilde{u}\to u_e(x)=bx,\ \tilde{T}\to\tilde{T}_\infty,\ \tilde{C}\to\tilde{C}_\infty\text{ as }y\to\infty \tag{5}$$

Implementing [40]:

$$\tilde{v}=-\sqrt{a\nu}f\left(\eta\right),\quad \tilde{u}=axf'\left(\eta\right),\quad \theta\left(\eta\right)=\frac{\tilde{T}-\tilde{T}_\infty}{\tilde{T}_w-\tilde{T}_\infty}$$
$$\eta=\sqrt{\frac{a}{\nu}}y,\quad \phi\left(\eta\right)=\frac{\tilde{C}-\tilde{C}_\infty}{\tilde{C}_w-\tilde{C}_\infty} \tag{6}$$

The flow expressions take the following form:

$$f'''+\left(1+\lambda_2\right)\left[ff''-f'^2+\text{Ha}\left(A-f'\right)+A^2\right]+\beta\left(f''^2-ff^{(iv)}\right)+$$
$$+\left(\frac{1+\lambda_2}{\text{Re}_x^2}\right)\left[\text{Gr}\left(1+\beta_t\theta\right)\theta+\text{Gr}^*\left(1+\beta_c\phi\right)\right]=0 \tag{7}$$

$$\left(1+\lambda_2\right)\theta''+\Pr\left(1+\lambda_2\right)\left[f\theta'+Nb\theta'\phi'+Nt\theta'^2+\delta\theta+\text{EcHa}f'^2\right]+$$
$$+Tr\left(1+\lambda_2\right)\left[3\left(T_c+\theta\right)^2\theta'^2+\left(T_c+\theta\right)^3\theta''\right]+\Pr\text{Ec}\left[f''+\beta f''\left(f'f''-ff'''\right)\right] \tag{8}$$

$$\frac{1}{\text{Sc}}\phi''+f\phi'+\frac{1}{\text{Sc}}\frac{Nt}{Nb}\theta''+\gamma\phi\left(1+\frac{\theta}{T_c}\right)\exp\left(-\frac{E}{\theta+T_c}\right)=0 \tag{9}$$

$$f(0)=0,\quad f'(0)=1,\quad Nb\phi'(0)+Nt\theta'(0)=0,\quad \theta'(0)=-\beta_i\left[1-\theta(0)\right]$$
$$f'(\infty)\to A,\quad \phi(\infty)\to 0,\quad \theta(\infty)\to 0 \tag{10}$$

In the aforementioned expressions:

$\text{Ha}=\dfrac{\sigma B_0^2}{a\rho}$ represents Hartmann number

$\beta=a\lambda_1$ material variable

$A=\dfrac{b}{a}$ ratio parameter

$Tr=\dfrac{16\sigma^0(\tilde{T}_w-\tilde{T}_\infty)^3}{3kk^0}$ radiation variable

$\beta_t=\dfrac{\chi_2(\tilde{T}_w-T_\infty)}{\chi_1}$ convection variable due to temperature

$\text{Re}_x=\dfrac{ax^2}{\nu}$ local Reynolds number

$\beta_c=\dfrac{\chi_4\tilde{C}_\infty}{\chi_3}$ convection variable due to concentration

$$\mathrm{Gr}^* = \frac{g\chi_3 \tilde{C}_\infty x^3}{\nu^2} \quad \text{Grashof number due to concentration}$$

$$\mathrm{Gr} = \frac{g\chi_1 (\tilde{T}_w - \tilde{T}_\infty) x^3}{\nu^2} \quad \text{Grashof number due to temperature}$$

$$\mathrm{Pr} = \frac{\mu c_p}{k} \quad \text{Prandtl number}$$

$$Nt = \frac{\tau D_T (\tilde{T}_w - \tilde{T}_\infty)}{\nu \tilde{T}_\infty} \quad \text{the thermophoresis parameter}$$

$$\mathrm{Ec} = \frac{a^2 x^2}{c_p (\tilde{T}_w - T_\infty)} \quad \text{the Eckert number}$$

$$Nb = \frac{\tau D_B \tilde{C}_\infty}{\nu} \quad \text{Brownian motion parameter}$$

$$T_c = \frac{\tilde{T}_\infty}{\tilde{T}_w - \tilde{T}_\infty} \quad \text{dimensionless temperature}$$

$$\gamma = \frac{k_r^2}{a} \quad \text{reaction rate}$$

$$\mathrm{Sc} = \frac{\nu}{D_B} \quad \text{Schmidt number}$$

$$\delta = \frac{Q_0}{a \rho c_p} \quad \text{heat source/sink variable}$$

$$E = \frac{E_a}{\kappa (\tilde{T}_w - \tilde{T}_\infty)} \quad \text{denotes the dimensionless activation energy}$$

$$\beta_i = \frac{h_f}{k} \sqrt{\frac{\nu}{a}} \quad \text{Biot number}$$

Physical quantities

Skin friction coefficient (surface drag force)

Mathematically, it is defined:

$$C_{fx} = \frac{-2\tau_w}{\rho u_w^2} \tag{11}$$

where τ_w denotes the wall shear stress and defined:

$$\tau_w = \frac{\mu}{1+\lambda_2} \left[\frac{\partial u}{\partial y} + \lambda_1 \left(u \frac{\partial^2 u}{\partial x \partial y} + v \frac{\partial^2 u}{\partial y^2} \right) \right]_{y=0} \tag{12}$$

Putting eq. (13) in eq. (12):

$$C_{fx} \left(\mathrm{Re}_x \right)^{0.5} = -\frac{2}{1+\lambda_2} f''(0) + \beta \left[f'(0) f''(0) - f(0) f'''(0) \right] \tag{13}$$

Heat transfer rate (Nusselt number)

We have:

$$\mathrm{Nu}_x = \frac{xq_w}{k\left(\tilde{T}_w - \tilde{T}_\infty\right)} \tag{14}$$

where q_w represents the wall heat flux and mathematically expressed

$$q_w = -\left[k\left(1+\frac{16\sigma^o\tilde{T}^3}{3kk^o}\right)\frac{\partial\tilde{T}}{\partial y}\right] \tag{15}$$

Invoking eq. (16) in eq. (15), we have:

$$\mathrm{Nu}_x\,\mathrm{Re}^{-0.5} = -\left[1+T_r\left(\theta(0)+T_c\right)^3\right]\theta'(0) \tag{16}$$

Sherwood number (mass transfer rate)

It is defined:

$$\mathrm{Sh}_x = \frac{xJ_w}{D_B\tilde{C}_\infty} \tag{17}$$

where J_w indicates the wall mass flux and mathematically:

$$J_w = -D_B\left[\frac{\partial\tilde{C}}{\partial y}\right]_{y=0} \tag{18}$$

From eqs. (19) and (18), we get:

$$\mathrm{Sh}_x\,\mathrm{Re}^{-0.5} = -\phi'(0) \tag{19}$$

where $\mathrm{Re}_x = ax^2/\nu$ signifies the local Reynolds number, C_{fx} – the skin friction coefficient, Nu_x – the Nusselt number, and Sh_x – the Sherwood number.

The homotopy analysis method solution

In order to obtained the series solutions of non-linear OPE by homotopy analysis method it is compulsory to define the linear operator and initial guesses. The linear operator and initial guesses for momentum, temperature and nanoparticles concentration are defined:

$$\begin{gathered} f_0(\eta) = 1 - A(1-\eta) - (1-A)\exp(-\eta) \\ \theta_0(\eta) = \frac{\beta_i}{1+\beta_i}\exp(-\eta) \\ \theta_0(\eta) = \frac{\beta_i}{1+\beta_i}\left(\frac{Nt}{Nb}\right)\exp(-\eta) \end{gathered} \tag{20}$$

$$\left.\begin{aligned} L_f &= \frac{\mathrm{d}^3}{\mathrm{d}\eta^3} - \frac{\mathrm{d}}{\mathrm{d}\eta} \\ L_\theta &= \frac{\mathrm{d}^2}{\mathrm{d}\eta^2} - 1 \\ L_\phi &= \frac{\mathrm{d}^2}{\mathrm{d}\eta^2} - 1 \end{aligned}\right\} \tag{21}$$

with

$$\begin{aligned} L_f\left[c_1 + c_2 \exp(-\eta) + c_3 \exp(\eta)\right] &= 0 \\ L_\theta\left[c_4 \exp(-\eta) + c_5 \exp(\eta)\right] &= 0 \\ L_\phi\left[c_6 \exp(-\eta) + c_6 \exp(\eta)\right] &= 0 \end{aligned} \tag{22}$$

in which c_i(1)-(7) signifies the arbitrary constant.

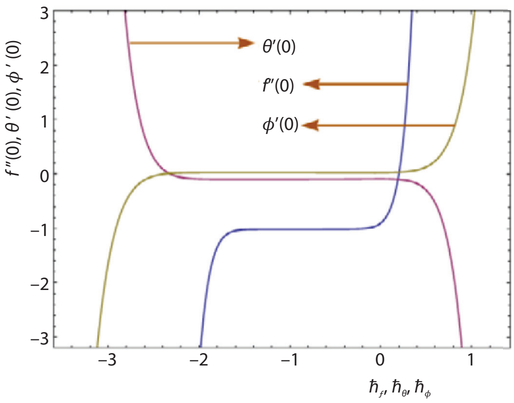

Figure 2. The $\hbar$-curves for $f(\eta)$, $\theta(\eta)$, and $\phi(\eta)$

Convergence analysis

The auxiliary variables $\hbar_f$, $\hbar_\theta$, and $\hbar_\phi$ plays a noteworthy role in convergence series solutions. These variables control and adjust the convergent portion of series solutions. The $\hbar$ is the curves for momentum, temperature, and nanoparticles volume concentration are plotted in fig. 2. It has been examined that the suitable estimations for $f(\eta)$, $\theta(\eta)$, and $\phi(\eta)$ are $-1.82 \le \hbar_f \le 0.21$, $-2.01 \le \hbar_\theta \le 0.21$, and $-2.1 \le \hbar_\phi \le 0.15$. Table 1 is constructed for the convergence of series solutions when $Nb = 0.7$, $\delta = T_c = 0.5$, $\lambda_2 = n = \beta = E = \gamma = A = 0.1$, $Nt = 0.2$, $\mathrm{Gr} = \mathrm{Gr}^* = 0.4$, $\mathrm{Ha} = \beta_t = \beta_i = 0.2$, $\beta_c = E = 0.3$, $\mathrm{Pr} = \mathrm{Sc} = 1.0$, and $Tr = 0.4$.

Table 1. Numerical results for momentum, temperature and nanoparticles volume concentration

Order of approximation	$-f''(0)$	$-\theta'(0)$	$-\phi'(0)$
1	1.061	0.0889	0.0254
10	0.0832	0.0832	0.0238
20	0.0786	0.0786	0.0224
30	0.0773	0.0777	0.0221
35	0.0773	0.0777	0.0221
45	0.0773	0.0777	0.0221

Discussion

In this section we examined the effects of flow variables on velocity, concentration, temperature, skin friction coefficient, Sherwood and Nussels numbers. Figures 3-7 examined the behavior of A, β, Gr, Gr^*, and Ha on velocity, $f'(\eta)$. Impact of A on $f'(\eta)$, is presented in fig. 3. It is noted that, $f'(\eta)$, enhances for larger A. Figure 4 depict the influence of β on $f'(\eta)$. For larger estimation of β velocity show decreasing behavior. Physically β is the relation of relaxation observation times. By increase in β relaxation time is higher and generates more resistance to flow due to which, $f'(\eta)$, reduces. Figure 5 captured the effect of Gr on $f'(\eta)$. Clearly, $f'(\eta)$, is increasing function of β. The outcome of $f'(\eta)$, with variation of Gr^* is described in fig. 6. The $f'(\eta)$ decreased through Gr^*. Figure 7 is sketched for $f'(\eta)$ with variation in Ha. This figure show that, $f'(\eta)$, is decays for higher estimation of Ha. Physically Ha is an increasing function of resistive force (Lorentz force) therefore, $f'(\eta)$ diminished. Figures 8-13 described the influences of

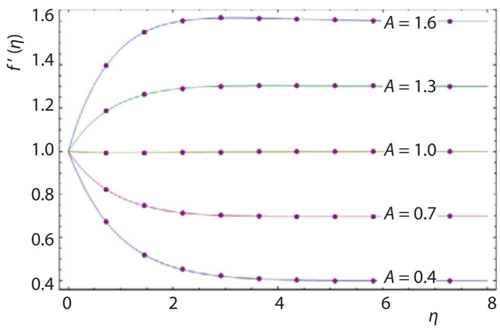

Figure 3. The $f'(\eta)$ via A

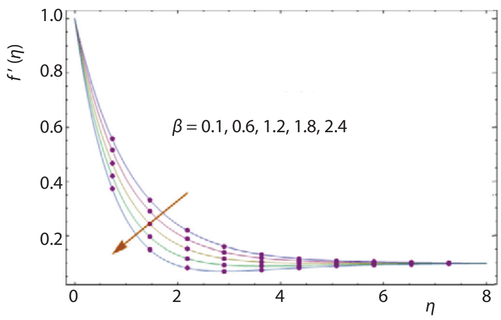

Figure 4. The $f'(\eta)$ via β

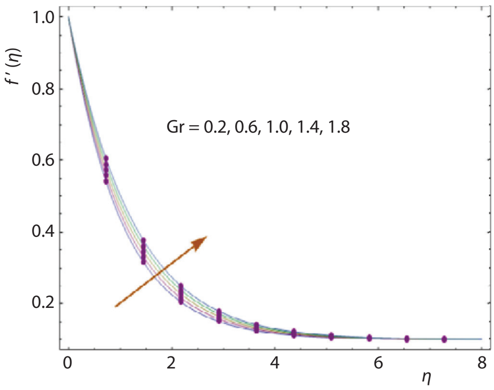

Figure 5. The $f'(\eta)$ via Gr

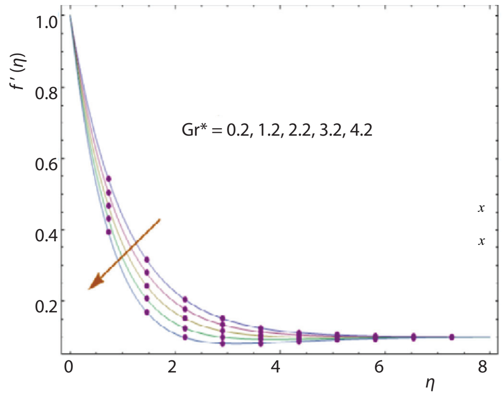

Figure 6. The $f'(\eta)$ via Gr*

Ha, β, Tr, Pr, Ec, and β_i on $\theta(\eta)$. Impact of Ha on $\theta(\eta)$ is plotted in fig. 8. It is noticed that $\theta(\eta)$ boosts via Ha. Figure 9 demonstrated the behavior of β on $\theta(\eta)$. The $\theta(\eta)$ enhances with larger variation in β. Figure 10 show the effect of Tr on $\theta(\eta)$. For higher values of Tr temperature is enhanced. Variation of $\theta(\eta)$ through Pr is portrayed in fig. 11. The $\theta(\eta)$ is decreasing function of Pr. Figure 12 is focused to describe the impact of Ec on $\theta(\eta)$. Clearly $\theta(\eta)$ boosts for larger estimation of Ec. Figure 13 captured the influence of β_i on $\theta(\eta)$. This figure show that $\theta(\eta)$ enhanced for larger values of β_i. Figures 14-18 disclosed the characteristics of γ, Sc, Nt, Nb, and E on $\phi(\eta)$. Impact of γ on $\phi(\eta)$ is portrayed in fig. 14. It is noticed that $\phi(\eta)$ is dominant for higher values of. Figure 15 sketched for $\phi(\eta)$ through variation in Sc. The $\phi(\eta)$ boosts with Sc. Figure 16 captured the impact of Nt on $\phi(\eta)$. Clearly $\phi(\eta)$ is a decreasing function of Nt. Variation of $\phi(\eta)$ through Nb is presented in fig. 17. The $\phi(\eta)$ is dominant for larger values of Nb. Figure 18 depict the characteristic of E on $\phi(\eta)$. The $\phi(\eta)$ boosts via E. The effects of β, Ha, Gr, and Gr* on C_{fx} are presented in figs. 19 and 20. In these figures we noted that C_{fx} is boosts via β, Ha, and Gr* while reduces through Gr. Influences of Ha, β, Pr, and Ec on Nu$_x$ are reported in figs. 21 and 22. Clearly Nu$_x$ is a decreasing function of Ha and β however enhanced with Pr and Ec. Characteristics of Nt, Nb, Ec, and T_c on Sh$_x$ are disclosed in figs. 23 and 24. It is noticed that Sh$_x$ is boosts via Nb and Tc while decays for larger values of Nt and Sc.

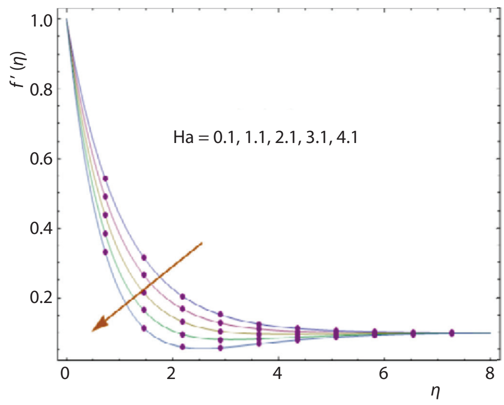

Figure 7. The $f'(\eta)$ via Ha

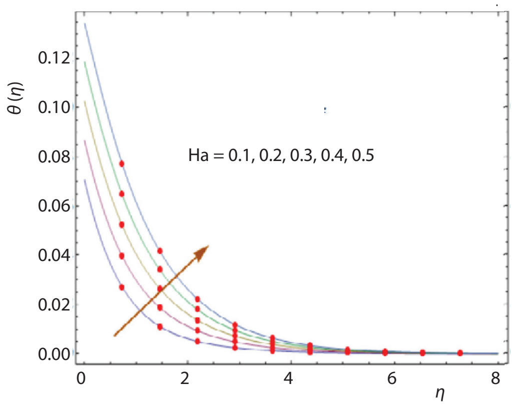

Figure 8. The $\theta(\eta)$ via Ha

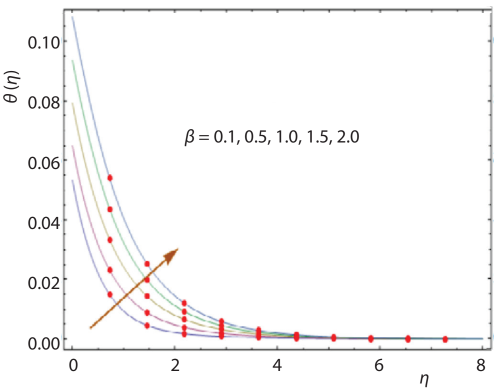

Figure 9.The $\theta(\eta)$ via β

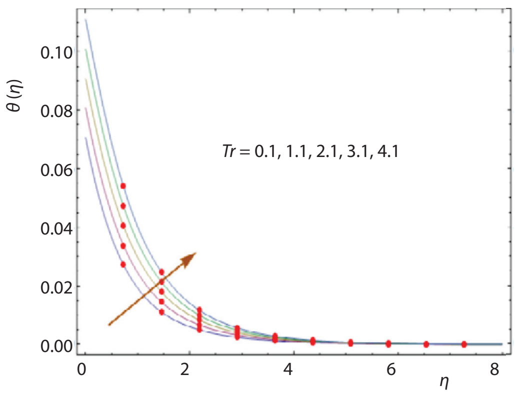

Figure 10. The $\theta(\eta)$ via *Tr*

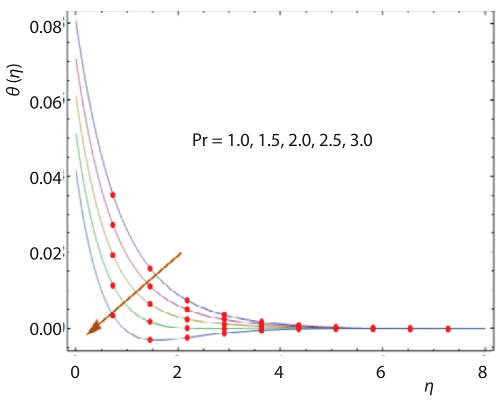

Figure 11. The $\theta(\eta)$ via Pr

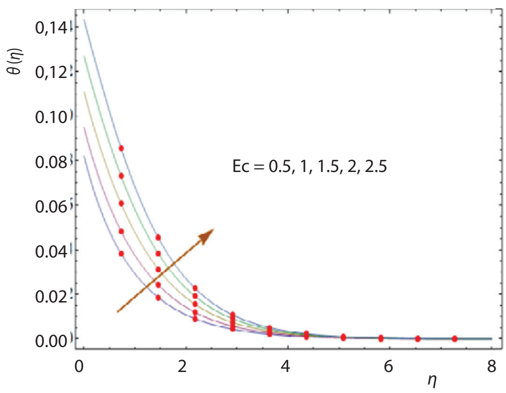

Figure 12. The $\theta(\eta)$ via Ec

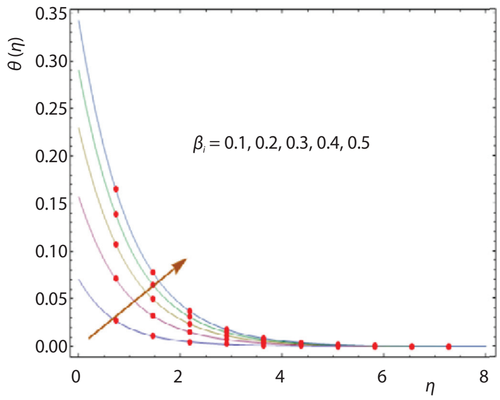

Figure 13. The $\theta(\eta)$ via β_i

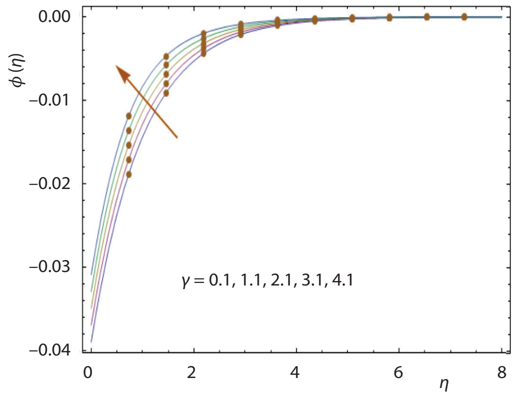

Figure 14. The $\phi(\eta)$ via γ

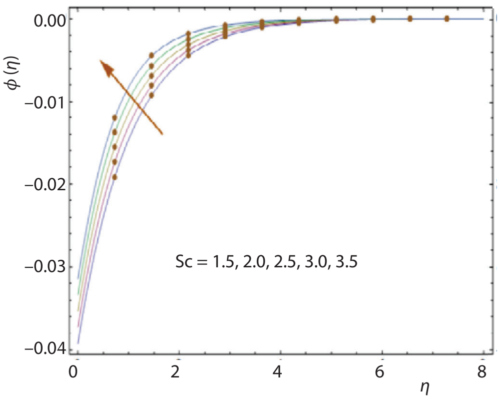

Figure 15. The $\phi(\eta)$ via Sc

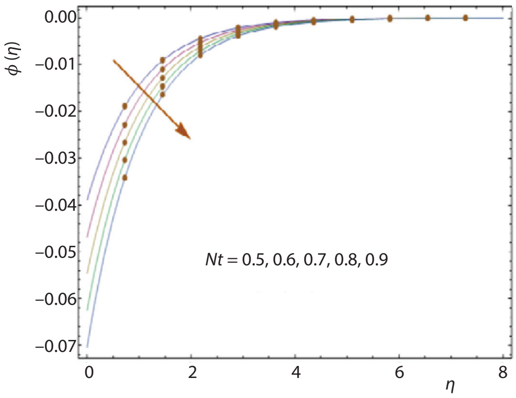

Figure 16. The $\phi(\eta)$ via Nt

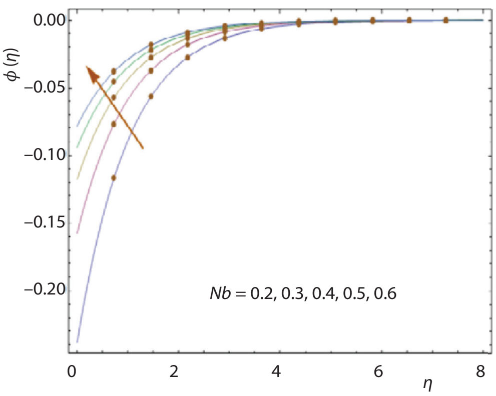

Figure 17. The $\phi(\eta)$ via Nb

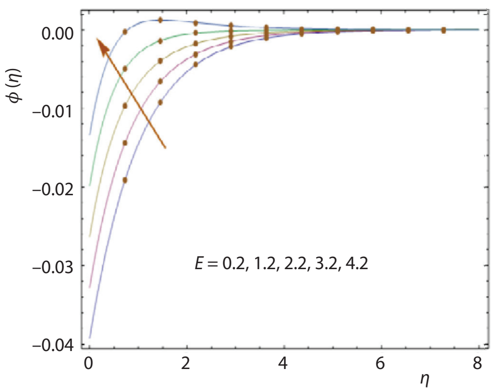

Figure 18. The $\phi(\eta)$ via E

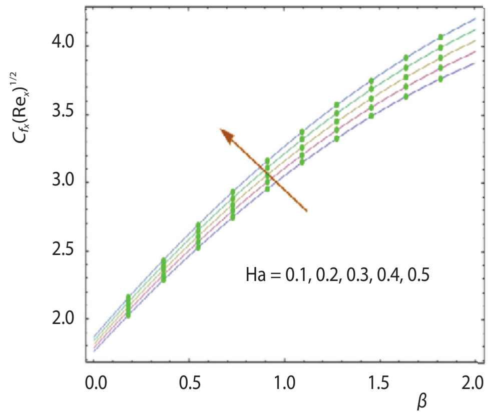

Figure 19. The C_{fx} via β and Ha

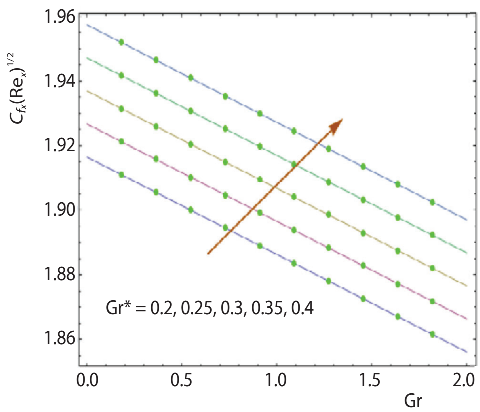

Figure 20. The C_{fx} via Gr and Gr*

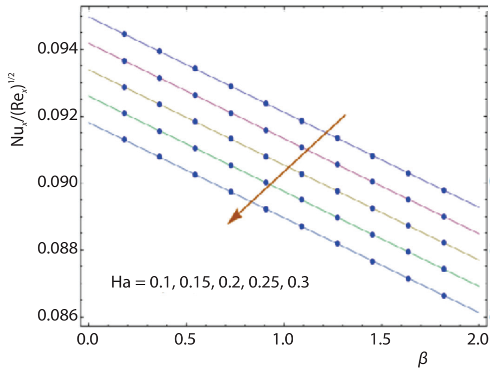

Figure 21. The Nu_x via β and Ha

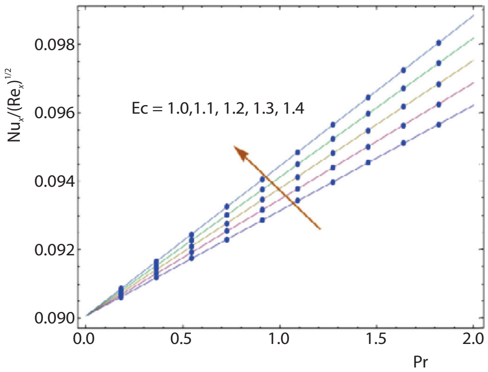

Figure 22. The Nu_x via Pr and Ec

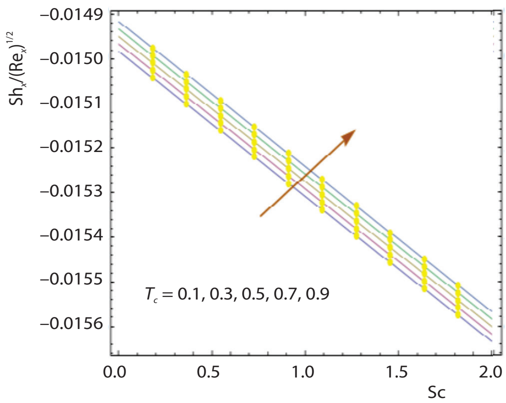

Figure 23. The Sh_x via *Nt* and *Nb*

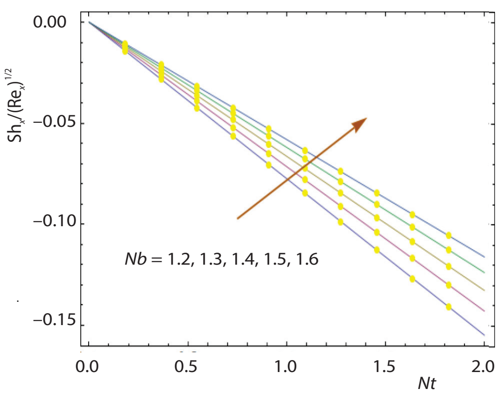

Figure 24. The Sh_x via Sc and T_c

Conclusions

Here we investigated the effects of activation energy, Joule heating, viscous dissipation, and magnetic field on mixed convective radiative flow of Jeffrey nanofluid over a sheet. Main outcomes are listed as follows.

- The $f'(\eta)$ is enhanced through A and Gr while decays with β, Ha, and Gr*.
- The $\theta(\eta)$ boosts via β, Ha, Tr, Ec, and β_i while reduces with Pr.
- The $\phi(\eta)$ is dominant for larger γ, Sc, Nb, and E however decreased through Nt.
- The C_{fx} and Nu$_x$ show opposite behavior against Ha and β.
- The Sh$_x$ increased for larger Nb and T_c while decreased with Nt and Sc.

Nomenclature

B_0 – strength of magnetic field
$\tilde{C}$ – concentracion
$\tilde{C}_\infty$ – ambient concentracion
c_p – specific heat
D_B – Brownian diffusion coefficient
D_T – thermophoresis diffusion coefficient
E_a – activation energy
h_f – coefficient of heat transport
k – thermal conductivity
k^0 – mean absorption
k_r – reaction rate
q_r – reaction rate
Q_0 – coefficient of heat source/sink
n – fitted rate constant
$\tilde{T}$ – temperature
$\tilde{T}_\infty$ – ambient temperaturue
u_e – free stream velocity
u_w – stretching velocity
$\tilde{u}$, $\tilde{v}$ – velocity components
x, y – space co-ordinates

Greek symbols

κ – Boltzmann constant
μ – dynamic viscosity
ν – kinematic viscosity
σ – electric conductivity
σ^0 – Stefan-Boltzmann coefficient
χ_1 – coefficient of linear thermal expansion
χ_2 – coefficient of non-linear thermal expansion
χ_3 – coefficient of linear concentration expansion
χ_4 – coefficient of non-linear concentration expansion

References

[1] Hayat, T., *et al*., Modelling and Analyzing Flow of Third Grade Nanofluid Due to Rotating Stretchable Disk with Chemical Reaction and Heat Source, Physica B*: Condensed Matter*, *537* (2018), May, pp. 116-126
[2] Turkyilmazoglu, M., Mixed Convection Flow of Magnetohydrodynamic Micropolar Fluid Due to a Porous Heated/Cooled Deformable Plate: *Exact solutions, International Journal of Heat and Mass Transfer*, *106* (2017), Mar., pp. 127-134
[3] Hayat, T., *et al*., Exploring Magnetic Dipole Contribution on Radiative Flow of Ferromagnetic Williamson Fluid, *Results in Physics*, *8* (2018), Mar., pp. 545-551
[4] Kumar, R., *et al*., Radiative Heat Transfer Study for Flow of Non-Newtonian Nanofluid Past a Riga Plate with Variable Thickness, *Journal of Molecular Liquids*, *248* (2017), Dec., pp. 143-152
[5] Hayat, T., *et al*., Non-Darcy Forchheimer Flow of Ferromagnetic Second Grade Fluid, *Results in Physics*, *7* (2017), Sept., pp. 3419-3424
[6] Thammanna, G. T., *et al*., The 3-D MHD Flow of Couple Stress Casson Fluid Past an Unsteady Stretching Surface with Chemical Reaction, *Results in Physics*, *7* (2017), Oct., pp. 4104-4110
[7] Kumar, K. G., Effects of mass transfer on MHD 3-D flow of a Prandtl liquid over a flat plate in the presence of chemical reaction, *Results in Physics*, *7* (2017), Sept., pp. 3465-3471
[8] Kumar, K. G., *et al*., Impact of Chemical Reaction on Marangoni Boundary-Layer Flow of a Casson Nanoliquid in the Presence of Uniform Heat Source Sink, *Diffusion Foundations*, *11* (2017), Aug., pp. 22-32
[9] Abbasi, F. M., *et al*., Mixed Convection Flow of Jeffrey Nanofluid with Thermal Radiation and Double Stratification, *Journal of Hydrodynamics*, *Ser. B*, *28* (2016) 5, pp. 840-849
[10] Javed, M. F., *et al*., Axisymmetric Flow of Casson Fluid by a Swirling Cylinder, *Results in Physics*, *9* (2018), Apr., pp. 1250-1255
[11] Khan, N. B., *et al*., Numerical Investigation of Vortex-Induced Vibration of an Elastically Mounted Circular Cylinder with One-Degree of Freedom at High Reynolds Number Using Different Turbulent Models, *Proceedings of the Institution of Mechanical Engineers – Part M*: *Journal of Engineering for the Maritime Environment*, *233* (2018), 2, pp. 443-453
[12] Hayat, T., *et al*., Heat and Mass Transfer Analysis in the Stagnation Region of Maxwell Fluid with Chemical Reaction over a Stretched Surface, *Journal of Thermal Science and Engineering Applications*, *10* (2018), 1, 011002

[13] Khan, N. B., *et al*., Numerical Investigation of the Vortex-Induced Vibration of an Elastically Mounted Circular Cylinder at High Reynolds Number (Re = 10^4) and Low Mass Ratio Using the RANS Code, *Plos One*, *12* (2017), Oct., e0185832
[14] Khan, N. B., *et al*., The VIV Study of an Elastically Mounted Cylinder Having Low Mass-Damping Ratio Using RANS Model, *International Journal of Heat and Mass Transfer*, *121* (2018), June, pp. 309-314
[15] Shehzad, S. A., *et al*., The 3-D Flow of Jeffery Fluid with Convective Surface Boundary Conditions, *International Journal of Heat and Mass Transfer*, *55* (2012), S15-16, pp. 3971-3976
[16] Turkyilmazoglu, M., Pop I., Exact Analytical Solutions for the Flow and Heat Transfer Near the Stagnation Point on a Stretching/Shrinking Sheet in a Jeffrey Fluid, *International Journal of Heat and Mass Transfer*, *57* (2013), 1, pp. 82-88
[17] Khan, M., *et al*., Thermal and Concentration Diffusion in Jeffery Nanofluid-Flow over an Inclined Stretching Sheet: A Generalized Fourier's and Fick's Perspective, *Journal of Molecular Liquids*, *251* (2018), Feb., pp. 7-14
[18] Hayat, T., *et al*., The 3-D Flow of a Jeffery Fluid over a Linearly Stretching Sheet, *Communications in Non-Linear Science and Numerical Simulatio*, *17* (2012), 2, pp. 699-707
[19] Ojjela, O., Influence of Thermophoresis and Induced Magnetic Field on Chemically Reacting Mixed Convective Flow of Jeffrey Fluid between Porous Parallel Plates, *Journal of Molecular Liquids*, *232* (2017), Apr., pp. 195-206
[20] Rudraswamy, N. G., *et al*., Combined Effect of Joule Heating and Viscous Dissipation on MHD 3-D Flow of a Jeffrey Nanofluid, *Journal of Nanofluids*, *6* (2017), 2, pp. 300-310
[21] Kumar, K. G., *et al*., Influence of Non-Linear Thermal Radiation and Viscous Dissipation on 3-D Flow of Jeffrey Nanofluid over a Stretching Sheet in the Presence of Joule Heating, *Non-Linear Engineering, 6* (2017), 3, pp. 207-219
[22] Rudraswamy, N. G., *et al*., Soret and Dufour Effects in 3-D Flow of Jeffery Nanofluid in the Presence of Non-Linear Thermal Radiation, *Journal of Nanoengineering and Nanomanufacturing*, 6 (2016), 4, pp. 278-287
[23] Choi, S. U. S., Enhancing Thermal conductivity of fluids with nanoparticles developments and applications of non-Newtonian fluid-flow, *ASME FED*, *66* (1995), Jan., pp. 99-105
[24] Buongiorno, J., Convective Transfort in Nanofluids, *ASME Journal of Heat Transfer*, *128* (2006), 3, pp. 240-250
[25] Sheikholeslami, M., *et al*., Simulation of MHD CuO-Water Nanofluid-Flow and Convective Heat Transfer Considering Lorentz Forces, *Journal of Magnetism and Magnetic Materials*, *369* (2014), Nov., pp. 69-80
[26] Farooq, M., *et al*., The MHD Stagnation Point Flow of Viscoelastic Nanofluid with Non-Linear Radiation Effects, *Journal of Molecular Liquids*, *221* (2016), Sept., pp, 1097-1103
[27] Abbasi, F. M., Doubly Stratified Mixed Convection Flow of Maxwell Nanofluid with Heat Generation/Absorption, *Journal of Magnetism and Magnetic Materials*, *404* (2016), Apr., pp. 159-165
[28] Hayat, T., *et al*., Simulation of Ferromagnetic Nanomaterial Flow of Maxwell Fluid, *Results in Physics*, *8* (2018), Nov., pp. 34-40
[29] Lin, Y., *et al*., The MHD Pseudo-Plastic Nanofluid Unsteady Flow and Heat Transfer in a Finite Thin Film over Stretching Surface with Internal Heat Generation, *International Journal of Heat and Mass Transfer*, *84* (2015), May, pp. 903-911
[30] Zeeshan, A., *et al.*, Analysis of Activation Energy in Couette-Poiseuille Flow of Nanofluid in the Presence of Chemical Reaction and Convective Boundary Conditions, *Results in Physics*, *8* (2018), Mar., pp. 502-512
[31] Hayat, T., *et al*., Modelling Chemically Reactive Flow of Sutterby Nanofluid by a Rotating Disk in Presence of Heat Generation/Absorption, *Communications in Theoretical Physics*, *69* (2018), 5, pp. 569-576
[32] Hassan, M., *et al*., Convective Heat Transfer Flow of Nanofluid in a Porous Medium over Wavy Surface, *Physics Letters A*, *382* (2018), 38, pp. 2749-2753
[33] Hayat, T., *et al*., Entropy Generation in Darcy-Forchheimer Bidirectional Flow of Water-Based Carbon Nanotubes with Convective Boundary Conditions, *Journal of Molecular Liquids*, *265* (2018), Sept., pp. 629-638
[34] Shehzad, N., Electroosmotic Flow of MHD Power Law Al_2O_3-PVC Nanofluid in a Horizontal Channel: Couette-Poiseuille Flow Model, *Communications in Theoretical Physics*, *69* (2018), 6, pp. 655-666
[35] Ahmad, S., Entropy Generation Optimization and Unsteady Squeezing Flow of Viscous Fluid with Five Different Shapes of Nanoparticles, Colloids and Surfaces A: *Physicochemical and Engineering Aspects*, *554* (2018), Oct., pp. 197-210

[36] Hayat, T., *et al*., Investigation of Second Grade Fluid through Temperature Dependent Thermal Conductivity and non-Fourier Heat Flux, *Results in Physics*, *9* (2018), June, pp. 871-878
[37] Hayat, T., *et al*., A Frame Work for Heat Generation/Absorption and Modified Homogeneous-Heterogeneous Reaction in Flow Based on non-Darcy-Forchheimer Medium, *Nuclear Engineering and Technology*, *50* (2018), 3, pp. 389-395
[38] Hayat, T., *et al*., Magnetohydrodynamic Flow of Burgers Fluid with Heat Source and Power Law Heat Flux, *Chinese Journal of Physics*, *55* (2017), 2, pp. 318-330
[39] Qayyum, S., *et al*., Magnetohydrodynamic Non-Linear Convective Flow of Jeffrey Nanofluid over a Non-Linear Stretching Surface with Variable Thickness and Chemical Reaction, *International Journal of Mechanical Sciences*, *134* (2017), Dec., pp. 306-314
[40] Hayat, T., *et al*., Non-Linear Thermal Radiation Aspects in Stagnation Point Flow of Tangent Hyperbolic Nanofluid with Double Diffusive Convection, *Journal of Molecular Liquids*, *223* (2016), Nov., pp. 969-978

Paper submitted: May 24, 2018
Paper revised: July 20, 2018
Paper accepted: July 22, 2018